Enhanced Photon Extraction from a Nanowire Quantum Dot Using a Bottom-Up Photonic Shell

Mathieu Jeannin, Thibault Cremel, Teppo Häyrynen, Niels Gregersen, Edith Bellet-Amalric, Gilles Nogues, Kuntheak Kheng

Enhanced photon extraction from a nanowire quantum dot using a bottom-up photonic shell

Mathieu Jeannin,[1,*] Thibault Cremel,[2,*] Teppo Häyrynen,[3] Niels Gregersen,[3] Edith Bellet-Amalric,[2] Gilles Nogues,[1,†] and Kuntheak Kheng[2]

[1] *Univ. Grenoble Alpes, CNRS, Institut Néel, "Nanophysique et semiconducteurs" group, F-38000 Grenoble, France*

[2] *Univ. Grenoble Alpes, CEA, INAC, PHELIQS, "Nanophysique et semiconducteurs" group, F-38000 Grenoble, France*

[3] *DTU Fotonik, Department of Photonics Engineering, Technical University of Denmark, Ørsteds Plads, Building 343, DK-2800 Kongens Lyngby, Denmark*

Abstract

Semiconductor nanowires offer the possibility to grow high quality quantum dot heterostructures, and in particular CdSe quantum dots inserted in ZnSe nanowires have demonstrated the ability to emit single photons up to room temperature. In this letter, we demonstrate a bottom-up approach to fabricate a photonic fiber-like structure around such nanowire quantum dots by depositing an oxide shell using atomic layer deposition. Simulations suggest that the intensity collected in our NA=0.6 microscope objective can be increased by a factor 7 with respect to the bare nanowire case. Combining micro-photoluminescence, decay time measurements and numerical simulations, we obtain a 4-fold increase in the collected photoluminescence from the quantum dot. We show that this improvement is due to an increase of the quantum dot emission rate and a redirection of the emitted light. Our ex-situ fabrication technique allows a precise and reproducible fabrication on a large scale. Its improved extraction efficiency is compared to state of the art top-down devices.

* contributed equally to this work

† gilles.nogues@neel.cnrs.fr

I. INTRODUCTION

Controlling and enhancing the spontaneous emission of quantum emitters is one of the current key issues in the field of nanophotonics. Semiconductor quantum dots (QDs) are considered as promising and efficient single-photon emitters for quantum optics applications. [1–6] Over the past few years, several approaches have been pursued to control their emission properties, from the use of photonic crystals [7, 8] to top-down photonic wires [9–11] and trumpets.[12, 13] These strategies are based on the early work of Purcell[14] which demonstrated that the spontaneous emission of an emitter can be modified by engineering its electromagnetic environment. They rely on a waveguiding approach to increase the coupling between a well-defined propagating optical mode and the QD while simultaneously reducing the coupling between the QD and background radiation modes, offering control of both the optical mode profile and the QD spontaneous emission rate.

In this context, the interest of the dot-in-a-nanowire configuration fabricated using bottom-up methods naturally arises because it provides a simple way to ensure the centering of a single quantum emitter in the photonic structure.[15–17] The bottom-up fabrication method also avoids heavy processing, like etching the semiconducting material, that is often detrimental to the QDs optical properties. However, the main realizations up to now concern III-V semiconductors, [15–17] limiting the operation range to the cryogenic temperature. Tackling this issue, the potential of II-VI materials, in particular CdSe QDs inserted inside ZnSe nanowires (NWs) has been demonstrated in previous studies. They allow for robust high temperature single-photon emission using heteroepitaxial [18] or homoepitaxial [19] nanowire growth. Contrary to all the aforementioned systems where the photonic wire structure has a diameter comparable to the wavelength λ/n of the guided light which allows for highly efficient coupling to the HE_{11} mode[20], the diameter of the II-VI NW embedding the QD ($\sim$20 nm) is much smaller than the wavelength of the emitted light (530 nm). It leads to light emission predominantly into non-guided radiation modes and a low collection efficiency. An additional fabrication effort has thus to be made to ensure an efficient coupling to the collection optics.

In a previous report[21] we have theoretically investigated the potential of using an oxide shell deposition on a bare ZnSe NW to form a thick photonic wire structure. In this article, we experimentally demonstrate the use of atomic layer deposition (ALD) to fabricate a

conformal aluminum oxide (Al_2O_3) shell around ZnSe NWs containing a single CdSe QD. We show that the oxide shell drastically enhances the light intensity emitted by the QD, and we use time-resolved microphotoluminescence to systematically study the effect of the shell thickness on the nanowire quantum dot (NWQD) emission rate. Our results are compared to numerical simulations accounting for the real NW geometry, evidencing the different physical mechanisms leading to the enhancement of the spontaneous emission from the QD and to the improved light collection from the emitting structure.

II. PRINCIPLES OF OPERATION

To illustrate the effect of the NW and its surrounding medium on the QD emission rate, let us consider a QD placed inside an infinitely long cylinder as illustrated in Fig. 1(a) radiating a field at a wavelength λ. The cylinder is made of a dielectric material (refractive index n) and has a diameter d. We first consider a dipole orientation perpendicular to the NW axis in order to use the NW as a propagation medium for the emitted light. In the limit where $d \ll \lambda/n$, the dielectric screening effect[11] reduces the spontaneous emission rate γ by a factor:

$$\frac{\gamma}{\gamma_0} = \frac{4}{n(n^2+1)^2}, \tag{1}$$

where γ_0 is the radiative emission rate in the bulk material of index n.[22] For a ZnSe cylinder ($n_{\mathrm{ZnSe}} = 2.68$ at λ=530 nm), the screening factor is $\sim$1/45. If the NW is surrounded by a shell of refractive index n_s instead of vacuum, equation 1 remains valid by replacing n with the index contrast n/n_s. For an Al_2O_3 surrounding medium (n_s =1.77), the screening factor becomes $\sim$1/4.1, resulting in an order of magnitude larger radiative rate.

In addition to changing the dielectric screening, the Al_2O_3 shell also influences the guiding of light along the NW. We have computed the total emission rate γ and the emission rate γ_{HE11} into the fundamental HE_{11} waveguide mode from a radial dipole as function of the shell thickness t_s [see Fig. 1(a)] using a semi-analytical approach[23] combined with an efficient non-uniform discretization scheme in k space.[24] The results are plotted in Figure 1(b). We observe that the shell thickness of $\sim$120 nm not only leads to an increased total emission rate, it also allows for confinement of the fundamental HE_{11} mode to the core-shell NW leading to a preferential coupling of the emitted light to this mode. Figure 1(c) presents the spontaneous emission β factor representing the fraction $\beta = \gamma_{\mathrm{HE11}}/\gamma$ of emitted light coupled

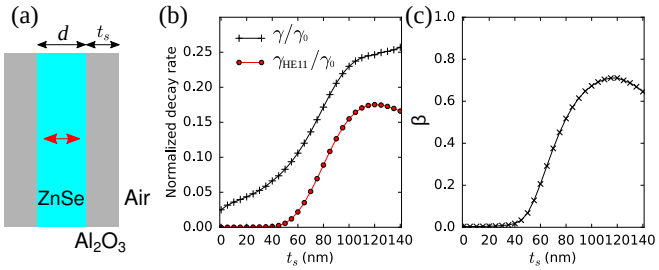

Figure 1. (a) Geometry of the infinite NW. (b) Total spontaneous emission rate (black +) and spontaneous emission rate into the first guided mode HE_{11} (red •) as a function of shell radius for a radial dipole. (c) Fraction β of power radiated into the HE_{11} mode.

to the HE_{11} mode. We observe indeed that up to 71% of the emitted light is coupled to this mode for t_s=120 nm. The dipole thus becomes coupled to the equivalent of a monomode photonic wire[9–11, 15–17] paving the way to the control of its far-field radiation pattern.

III. SAMPLE FABRICATION

Our emitters are CdSe QDs embedded inside a ZnSe NW with a thin, epitaxial passivation $Zn_{0.83}Mg_{0.17}Se$ shell grown around the NW. They are grown by molecular beam epitaxy on a GaAs(111)B substrate. A ZnSe buffer layer is first grown on the GaAs substrate after which a thin layer of Au (less than one monolayer thick) is evaporated on the sample surface and dewetted at 510 °C to form small (∼10 nm diameter) Au droplets that serve as a catalyst for the NW growth. The substrate temperature is then set at 400 °C and a flux of Zn and Se atoms with an excess of Se is used, inducing preferential growth of vertical ZnSe NWs. The NWs are in wurtzite phase and their diameter is the same as the droplet (∼10 nm diameter). The thickness of the initial Au layer is chosen to ensure a low NW density ($\leq$ 1 NW per μm^2). After the growth of a 400 nm high NW, the atom fluxes are stopped to allow the evacuation of residual Se atoms inside the droplet. Then, the QD is grown under a flux of Cd and Se atoms for 20 s. The fluxes are interrupted again before the ZnSe growth is resumed, resulting in an expected QD height of 2-3 nm inserted in a ∼700 nm high NW. Finally, an epitaxial $Zn_{0.83}Mg_{0.17}Se$ shell (5 nm thick) is grown around the NW at 220 °C. A scanning electron microscope (SEM) image of such a CdSe/ZnSe/ZnMgSe core/shell NWQD system is presented in Figure 2(a). The flag-shape termination of the NW is formed during the

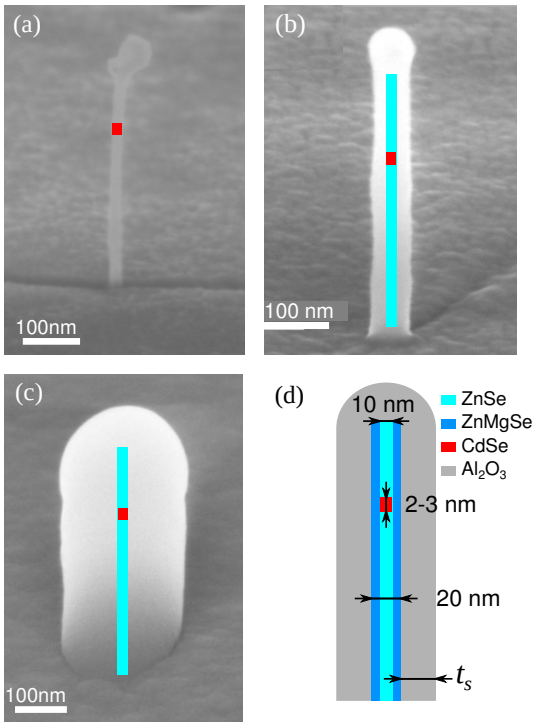

Figure 2. (a) SEM image of a standing ZnSe/ZnMgSe NW embedding a CdSe QD. The QD position is marked by the red square. (b,c) Tilted SEM image of a ZnSe NW after a 20 nm and 110 nm thick Al_2O_3 shell deposition respectively. The NW is sketched on the SEM image. Note the circular shape of the shell as well as its hemispherical termination above the NW apex. (d) Sketch of the NWQD geometry, indicating the QD height (2-3 nm), the NW diameter ($\simeq$10 nm), the epitaxial shell thickness ($\simeq$5 nm) and the ALD shell thickness t_s.

growth of the ZnMgSe shell. It is present in some NWs.

The higher bandgap of $Zn_{0.83}Mg_{0.17}Se$ shell prevents the charge carriers to recombine non-radiatively on the ZnSe NW sidewall and hence improves the quantum yield of the CdSe emitter. In principle, it could directly be used to grow a photonic wire of diameter $\sim \lambda/n_{\mathrm{ZnSe}}$ around the NWQD. However, during the epitaxial shell growth two phenomena are competing: the radial growth of the shell around the wurtzite NWs, and the vertical growth of a 2D $Zn_{0.83}Mg_{0.17}Se$ layer on the sample surface. The radial shell growth rate is very low because the growth of ZnSe on WZ surfaces is not favourable. Because of this low shell growth rate, a trade-off has to be found to avoid burying the NWs in a $Zn_{0.83}Mg_{0.17}Se$ matrix. As a result, only thin epitaxial shells can be fabricated.

The complexity of creating a thick epitaxial shell is one of the reasons why we fabricate

the photonic structure by depositing an oxide shell around the NW using ALD. Another reason is that, since this process step can be done *separately* from the NW growth process, it allows to tune ex situ the shell parameters after a first optical characterization of the QD. Indeed, due to its slow deposition rate, the ALD process allows to precisely control the deposited thickness, which can also be finally verified using scanning electron microscopy. We have tested several oxide materials, and selected Al_2O_3 because it produced very smooth and conformal, amorphous shells. Figure 2(b) and (c) show two SEM images of the resulting oxide shell deposition (20 nm and 110 nm), and the complete structure is sketched in Fig. 2(d). We note that the conformal deposition allows to end the NW+shell structure by an almost perfect half-sphere as can be seen in Fig. 2(b,c). ALD also buries the Au droplet under the shell. The latter might interact with the field emitted by the QD through its localized plasmon resonance. Considering its small diameter it will essentially absorb the incoming field. Moreover the guided HE11 mode profile presents a minimum on the NW axis. This is why we neglect the droplet influence in the following.

IV. EXPERIMENTAL RESULTS

A sample from a single epitaxial growth process is cut in pieces, and photonic structures with different oxide shell thicknesses are fabricated. Taking advantage of the low NW density, individual structures are optically characterized directly on the growth substrate. The samples are mounted on the cold finger of a He-flux cryostat and cooled down to 4 K. Individual photonic structures are probed using confocal microphotoluminescence (µPL). They are excitated by a supercontinuum pulsed laser (Fianium WhiteLase, 10 ps pulse duration, repetiton rate 76 MHz) and a spectrometer selecting a 10 nm bandwidth centered around 485 nm. This excitation energy, below the ZnSe gap, allows us to induce crossed transitions between delocalized states in the NW 1D continuum and a discrete confined 0D state in the NWQD band structure[25]. In this configuration, the NW axis is aligned with the optical axis and emission from the QD is collected by a $NA = 0.6$ objective. A typical NWQD spectrum is presented in Figure 3(a) as a function of the pump laser power. Three lines can be identified and are attributed to the exciton (X), the charged exciton (CX) and the bi-exciton (XX) respectively. The total emission intensity of the X line as a function of the pump power is reported in Figure 3(b). It shows a linear increase at low pumping power, and

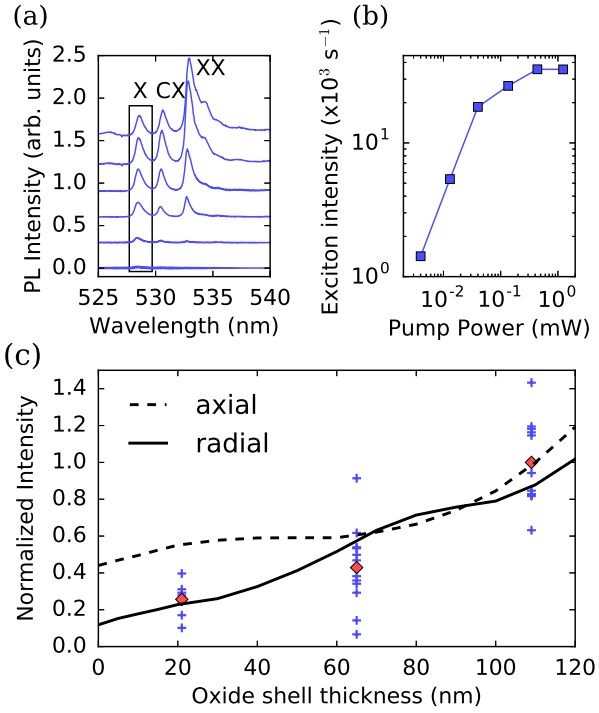

Figure 3. (a) µPL spectrum of a NWQD with 120 nm thick photonic shell for different pumping powers. It shows a exciton (X), charged exciton (CX) and biexciton (XX) lines. The corresponding pumping powers are reported in panel (b). The black rectangle indicates the integration bandwidth used to extract the total exciton emission intensity (X line). (b) Integrated exciton emission intensity as a function of pumping power, in a log-log scale. (c) Blue crosses: Total exciton emission intensity for different NWQDs as a function of the oxide shell radius. Red diamonds: average of the experimental data points. Data are normalized to the average intensity at t_s =110 nm Black lines: results of the numerical simulations for a radial (solid line) and an axial (dashed line) dipole. They are normalized to the axial intensity at t_s =110 nm

a constant plateau at high pumping powers corresponding to the saturation of the exciton level.[26] Under pulsed excitation, we note that changing the shell thickness might modify the laser power in the NW and the excitation probability of the QD. Hence if affects the slope at low power in Fig. 3(b). It has however no effect on the saturation plateau which only depends on the QD emission rate and light collection efficiency. This allows us to compare statistical sets of nanostructures with different oxide shell thicknesses. The total integrated emission at saturation as a function of the oxide shell thickness is reported in blue markers for each NWQD in Figure 3(c). The values have been normalized to the average intensity

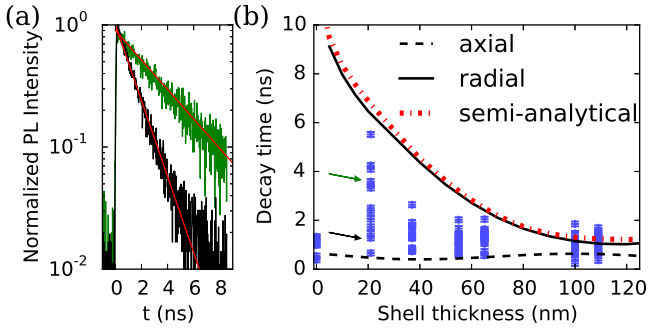

Figure 4. (a) Example of TRPL signal versus time for 2 NWs with a t_s=20 nm shell. Background counts are measured for $t < 0$ and substracted. Amplitude of counts are normalized to 1 to compare the 2 datasets. Red lines are mono-exponential fits, whose corresponding points in (b) are showm by arrows. (b) Blue crosses: experimental exciton decay times for several QDs as a function of the oxide shell radius. The vertical error bars represent the fit error. Black lines: numerical simulation results for a radial dipole (solid line), or an axial dipole (dashed line). Red dashed-dotted line: Semi-analytical calculations for the infinite NW.

at t_s =110 nm. For NWs without an oxide shell, the luminescence intensity is very low and we were never able to reach the saturation regime, this is why we do not report the corresponding points in Fig. 3(c). For each shell thickness, we observe a large spread in exciton saturation intensity. However, we note a general trend of increasing saturation intensity with increasing shell thickness, as demonstrated by the red markers which show the position of the average intensity of our measurements for each shell thickness. On average, the deposition of a 110 nm thick shell results in the experiments in an almost 4-fold enhancement of the collected intensity with respect to the 20 nm thick shell case. The semi-analytical calculations show that this enhancement is 10-fold when we compare to a NW without oxide shell.

The observed increase in intensity at saturation corresponds to the combination of improved collection efficiency through light redirection from the structure and enhancement of the spontaneous emission rate. In the latter case, a modification of the QD dynamics is expected to be detected by measuring the exciton decay rate. Time-resolved measurements were carried out using a low pump power as compared to the exciton saturation power to avoid any repopulation of the X level. The measured decay transients are thus monoexponential. The fitted decay constant is the total exciton decay time τ. The experiment

was carried out in another setup on a different set of photonic structures compared to the one of figure 3(c). The same excitation laser was used, the QD fluorescence was spectrally filtered in a spectrometer (500gr/mm grating) and integrated on an avalanche photodiode in a photon correlation setup, using the exit slit of the spectrometer as a spectral bandpass filter. The results of these measurements, presented in Figure 4 show also a great dispersion in decay time. One observes however that longer lifetimes are observed for smaller shell thickness (up to 5.9 ns). Increasing the shell thickness leads to an overall decrease in the measured exciton lifetime, hence an enhancement of the exciton decay rate in agreement with the results of the numerical simulations. For systems without an oxide shell, only a few NWQDs give a large enough signal to be properly measured. They yield a much smaller dispersion of short decay times.

V. DISCUSSION AND COMPARISON TO NUMERICAL SIMULATIONS

A. Dispersion of the results

For each oxide shell thickness, the large variations of the experimental results in both Figs. 3(c) and 4 have several possible origins. First, the presence of non-radiative recombination channels can reduce the intensity at saturation and change the decay time. The non-radiative recombination rate can vary from QD to QD because of fabrication inhomogeneities, leading to a spread in the measured values.[27] Second, variations in the QD aspect ratio and piezoelectric fields induced internal strain applied by both the ZnSe core and the $Zn_{0.83}Mg_{0.17}Se$ shell lead to different overlap of electron and hole wavefunctions and hence different exciton oscillator strengths. Finally, considering the QD aspect ratio and internal strain, we expect a heavy-hole exciton type for our QDs.[28–31] Heavy-hole exciton recombination results in a mixture of circularly polarized emission, composed of two degenerate out-of-phase radial dipoles. However, strain and confinement effects might lead to valence band mixing between light hole and heavy hole levels,[32–34] resulting in an emission composed of a mixture between axial and radial dipoles and hence to a spread in total emitted intensity, as we discuss later. Additional measurements on NWQDs grown in similar conditions and mechanically dispersed on a substrate (i.e. lying horizontally on it) revealed that one NWQD out of 6 emit light polarized along the NW axis, while others emit light polarized

perpendicularly to the NW axis, evidencing the presence of both kinds of dipoles. Due to the $Zn_{0.83}Mg_{0.17}Se$ shell and low temperature of observation, we expect that non-radiative effects play a minor role. The epitaxial shell prevents non-radiative decay channels owing to surface traps. Additional measurements as a function of temperature show that both the emission intensity and the decay time do not change significantly up to 150-200 K (not presented here). This indicates that the non-radiative effects are not dominating at low temperature, as in the present experiment. While we cannot yet completely rule out the contribution of non-radiative effects, we think that the major effect to explain the dispersion of the results comes from variations in valence band mixing and oscillator strength due to the local environment of the QD. Finally let us stress that the shortest decay times (1-2 ns) we measure remain longer than the decay time of CdSe self-assembled QD embedded in bulk ZnSe (<1 ns)[35]. The reduction of the dielectric screening effect is a main effect we evidence.

B. Collected intensity and radiative lifetime

To better understand the effect of the shell deposition on the NWQD emission, we perform numerical simulations of the photonic structure formed by the full NW + oxide shell geometry [see Fig. 2(d)]. It takes into account the presence of the ZnSe substrate, and the Al_2O_3 shell and layer deposited on the NWs and substrate. The QD is modeled as an oscillating electric dipole, either in the axial direction (along the NW axis) or in the radial direction (orthogonal to the NW axis). We perform finite-element method simulations (Comsol v4.1) to compute the total field radiated by the dipole.[34] For each shell thickness and dipole orientation, we evaluate the power radiated towards the objective by computing the flux of the Poynting vector over a surface limited by its numerical aperture (NA=0.6) in a region far from the NW where near field can be neglected. The results of these simulations are reported in Figure 3(c) in black lines for an axial (dashed line) or radial (solid line) dipole. The results are normalized to the axial intensity at t_s =110 nm. Comparing the simulated integrated intensity in the case of a 20 nm and 110 nm reveals an enhancement factor less than 2-fold for an axial dipole and almost 4-fold for a radial dipole. The 4-fold enhancement observed in our measurements suggests that on average, the dominant emitting dipole in our structure is radial, in good agreement with the recombination of a heavy hole exciton.

The theoretical limits for the radiative lifetimes is extracted from the numerical simulations by integrating the total power radiated over every direction for the two dipole orientations (radial and axial) P. We normalize this value by the same quantity computed for a dipole in bulk ZnSe P_0. For a purely radiative system we have $P/P_0 = \gamma/\gamma_0 = \tau_0/\tau$ [36], where τ and τ_0 are the radiative lifetime for the nanostructure and for bulk ZnSe respectively. Radiative times are presented in black lines in Figure 4, where we have chosen $\tau_0 = 300$ ps in good agreement with previously reported radiative lifetime of CdSe QD in bulk ZnSe[37]. The axial dipole radiates with an almost constant decay time as a function of the oxide shell thickness, while the radial dipole decay time strongly decreases with increasing oxide shell thickness t_s. Additionally, we compare the decay time for the radial dipole computed for the full geometry to the semi-analytical calculations for the infinite NW presented in fig. 1(b) with the same τ_0 value. The agreement is excellent indicating that interference effects due to reflections from the substrate and from the top hemispherical termination are negligible.

Comparing the trends of the simulations, we can confirm that our emitters bear a strong radial dipole character. The measurements dispersion can be well understood by considering that the real emitters are a mixture of radial and axial dipoles radiating with a characteristic decay time comprised between the simulated lifetimes of the pure radial and axial dipole. We do not observe long decay time for NWQDs without an oxide shell in Fig. 4. For these systems, it is very difficult to find emitters which are bright enough to be detected is because both the laser absorption and the emission rate of a radial dipole are very weak for such small NW diameters. We think that the emitters which have been selected correspond to NWQDs having a large fraction of axial dipole character as they are the brightest ones when no oxide shell is present.

C. Radiation pattern

To analyze the mechanisms leading to the increase in collected intensity with increasing shell thickness, we present in Figure 5 several simulated radiation patterns. They are represented as polar plots of the far-field intensity $I(\theta)$ in the top (x, z) plane, θ is the angle between the direction of observation and the vertical z axis. Simulations are made using respectively a radial dipole [along x, Figures 5(a-c)] or an axial dipole [along z, Figures 5(d-f)].

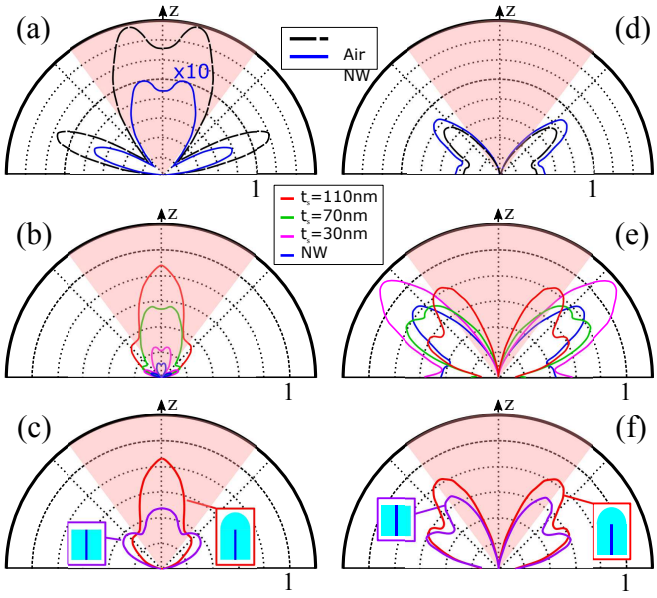

Figure 5. Radiation patterns from numerical simulations for a radial dipole placed at 470 nm above the substrate. The experimental NA region is shaded and indicated in red. (a,d) Comparison between the case of a free-standing emitter in air (black dashes), and embedded inside the NW (blue solid line) for a radial (a) or axial (d) dipole. They evidence the effect of the dielectric screening from the NW on the radial dipole and the absence of screening for the axial dipole. (b, e) Comparison of the total emitted intensity versus t_s for a radial (b) or axial (e) dipole. A combined effect of reduced dielectric screening and light guiding and redirection towards small angles is observed. (c, f) Effect of the shell layer termination shape for a radial (c) or axial (f) dipole. The hemispherical shape increases the fraction of light that is redirected towards the z direction.

Figures 5(a,d) show the effect of the NW structure alone (no oxide shell being present) on such dipoles by comparing it to the case of a free standing dipole in vacuum above the same ZnSe substrate. One can see that the presence of the NW does not affect the shape of radiation diagram, which is essentially determined by the interferences between the directly radiated field and its reflection on the substrate. Most remarkably, in the case of the radial dipole the presence of the NW dramatically reduces the emission intensity through the dielectric screening effect discussed earlier. Simulations show a radiative rate reduction by a factor $\sim 1/16 \simeq n_{\mathrm{ZnSe}}/45$ in agreement with the dielectric screening value predicted by Eq. (1). In contrast, in the case of the axial dipole it can be seen that the presence of the NW only slightly increases the emitted intensity.

Figures 5(b,e) show the computed radiation patterns of the NWQD for increasing oxide shell thickness t_s. In the case of the radial dipole, the shell first reduces the index contrast between the NW and the surrounding medium (cf. Eq. 1), resulting in a strong reduction of the emitter lifetime and thus in an increased total emitted intensity as seen in in Fig. 3(c) and Fig. 4. Note that the the intensity pattern shown in the polar plot must be multiplied by the solid angle $\sin\theta \mathrm{d}\theta$ if one wants to evaluate the power radiated in the numerical aperture. This is why the intensity for an axial dipole can be larger than for a radial one, as seen in Fig. 3(c). Second, as shown in Figure 1(c), the shell presence ensures preferential emission into the guided HE_{11} mode for increasing shell thickness. As a consequence a near-Gaussian far-field emission pattern corresponding to the far-field emission profile of the HE_{11} mode[38] is observed for t_s=110 nm, contrary to the structures with a smaller oxide shell thickness where one observes the presence of two closely-spaced lobes at small emission angles ($\pm 10^\circ$ with respect to the z-axis). The resulting emission into the 0.6 NA cone is maximum for t_s =110 nm, where the emission into the HE_{11} mode is nearly maximum [cf. Fig. 1(b)]. The effect of the oxide shell thickness on the axial dipole is completely different. While the total emitted intensity does not vary much, and hence the emitter lifetime stays constant (as noted in Fig. 4), the light emitted by the axial dipole does not couple to the HE_{11} mode but is emitted exclusively into radiation modes. Thus the fraction of intensity emitted towards the collection lens increases only slightly as the oxide shell thickness increases [cf. Fig.5(e)]. This intensity increase for the axial dipole also presented in Fig.3(c) is not due to a change in the spontaneous emission rate of the emitter, but rather to a slight redirection of the emitted light.

Finally, Figures 5(c,f)compare the actual hemispherical geometry of the oxide shell termination to the flat end of a simple lateral shell. They show that the presence of the hemisphere is beneficial to the radiation pattern for both kinds of dipole. For the radial dipole, the hemisphere enables a near-adiabatic expansion of the HE_{11} mode[38] leading to a narrowing of the far-field emission pattern and an increased collection by the numerical aperture. The axial dipole benefits less from the hemispherical termination of the photonic structure since no light from this dipole is coupled to the HE11 mode. We also note that half of the emitted light propagates towards the growth substrate and due to the index-matching condition between the NW and the substrate, this light is predominantly lost.

In order to assess the performances of our device we compute the ratio η between the

power radiated into a 0.6 NA to the one radiated into the top air side hemisphere. This parameter is a good figure of merit for the antenna redirection effect although it cannot be directly related to the overall collection efficiency because of the power lost in the substrate. For our full photonic structure and a radial dipole one has $\eta \simeq 80\%$ for t_s=110 nm. This value reduces to $\simeq 66\%$ for a flat terminated core-shell photonic wire illustrating the importance of the adiabatic expansion of the HE_{11} guided mode at the end of the wire. For the dipole in the NW without shell $\eta \simeq 55\%$. We have also simulated a structure inspired by state-of-the-art devices fabricated by top-down methods in Ref. [9]. In this case we simulate a 110 nm oxide shell photonic wire where the hemispherical termination is replaced by a conical tapper of Al_2O_3 whose radius progressively decreases from 120 to 10 nm in 1.5 μm. In this case one has $\eta \simeq 94\%$, showing that although beneficial our hemispherical termination is not optimal.

VI. CONCLUSION

In summary, we have presented a bottom-up approach to fabricate a dielectric antenna around a QD inserted inside a NW. This method allows for both reproducible and very precise fabrication of the structure on a large ensemble of emitters at once. It is based on the deposition of a thick oxide shell around the NW using atomic layer deposition. Experiments show a 4-fold enhancement of the QD photoluminescence shown in Fig. 3(c) between a 20 nm and a 110 nm thick shell. Semi-analytical calculations and numerical simulations of the structure reveal that the oxide shell thickness strongly acts on the radial dipole emission through two main phenomena: the reduction of the dielectric screening, which increases the spontaneous emission rate from the QD, and the redirection of light through a waveguiding effect. Simulations suggest that the collected intensity is multiplied by a factor 7 with respect to the bare NW case. The fabrication process of the photonic shell is very simple and can be applied to QDs emitting single photons up to room temperature. Although not optimal, the resulting structure is a step towards the best nanowire single photon sources operating at low temperature[9]. Dielectric screening could be further reduced by growing an oxide shell of higher index matching n_{ZnSe} like TiO_2. We note also that in our system a large fraction of the emitted power is radiated in the substrate. This loss channel could be reduced by having a mirror at the bottom of the structure.[15, 39] Moreover, to fully benefit from the waveguiding approach, a better control on the intrinsic QD properties has to be reached

to ensure the presence of radial dipoles, which radiate more efficiently in the experimental collection aperture.

ACKNOWLEDGMENTS

This work was supported by the French National Research Agency under the contract ANR-10-LABX-51-01 and the Danish Research Council for Technology and Production (LO-QIT Sapere Aude grant DFF #4005-00370).

[1] P. Michler, A. , Kiraz, C. Becher, W. V. Schoenfeld, P. M. Petroff, L. Zhang, E. Hu, and A. Imamoglu, "A quantum dot single-photon turnstile device," Science **290**, 2282–2285 (2000).

[2] Charles Santori, Matthew Pelton, Glenn Solomon, Yseulte Dale, and Yoshihisa Yamamoto, "Triggered single photons from a quantum dot," Phys. Rev. Lett. **86**, 1502 (2001).

[3] Charles Santori, David Fattal, Jelena Vučković, Glenn S. Solomon, and Yoshihisa Yamamoto, "Indistinguishable photons from a single-photon device," Nature **419**, 594–597 (2002).

[4] A. Zrenner, E. Beham, S. Stufler, F. Findeis, M. Bichler, and G. Abstreiter, "Coherent properties of a two-level system based on a quantum-dot photodiode," Nature **418**, 612–614 (2002).

[5] N. Akopian, N. H. Lindner, E. Poem, Y. Berlatzky, J. Avron, D. Gershoni, B. D. Gerardot, and P. M. Petroff, "Entangled photon pairs from semiconductor quantum dots," Phys. Rev. Lett. **96**, 130501 (2006).

[6] Andrew J. Shields, "Semiconductor quantum light sources," Nature Photon. **1**, 215 (2007).

[7] E. Viasnoff-Schwoob, C. Weisbuch, H. Benisty, S. Olivier, S. Varoutsis, I. Robert-Philip, R. Houdré, and C. J. M. Smith, "Spontaneous emission enhancement of quantum dots in a photonic crystal wire," Phys. Rev. Lett. **95**, 183901 (2005).

[8] T. Lund-Hansen, S. Stobbe, B. Julsgaard, H. Thyrrestrup, T. Sünner, M. Kamp, A. Forchel, and P. Lodahl, "Experimental realization of highly efficient broadband coupling of single quantum dots to a photonic crystal waveguide," Phys. Rev. Lett. **101**, 113903 (2008).

[9] Julien Claudon, Joël Bleuse, Nitin Singh Malik, Maela Bazin, P 'erine Jaffrennou, Niels Gregersen, Christophe Sauvan, Philippe Lalanne, and Jean-Michel Gérard, "A highly efficient single-photon source based on a quantum dot in a photonic nanowire,"

Nature Photon. **4**, 174–177 (2010).

[10] J. Heinrich, A. Huggenberger, T. Heindel, S. Reitzenstein, S. Höfling, L. Worschech, and A. Forchel, "Single photon emission from positioned GaAs/AlGaAs photonic nanowires," Appl. Phys. Lett. **96**, 211117 (2010).

[11] Joël Bleuse, Julien Claudon, Megan Creasey, Nitin. S. Malik, Jean-Michel Gérard, Ivan Maksymov, Jean-Paul Hugonin, and Philippe Lalanne, "Inhibition, enhancement, and control of spontaneous emission in photonic nanowires," Phys. Rev. Lett. **106**, 103601 (2011).

[12] Mathieu Munsch, Julien Claudon, Joël Bleuse, Nitin S. Malik, Emmanuel Dupuy, Jean-Michel Gérard, Yuntian Chen, Niels Gregersen, and Jesper Mørk, "Linearly polarized, single-mode spontaneous emission in a photonic nanowire," Phys. Rev. Lett. **108**, 077405 (2012).

[13] Mathieu Munsch, Nitin S. Malik, Emmanuel Dupuy, Adrien Delga, Joël Bleuse, Jean-Michel Gérard, Julien Claudon, Niels Gregersen, and Jesper Mørk, "Dielectric gaas antenna ensuring an efficient broadband coupling between an inas quantum dot and a gaussian optical beam," Phys. Rev. Lett. **110**, 177402 (2013).

[14] E.M. Purcell, "Spontaneous emission probabilities at radio frequencies," in *Proceedings of the American Physical Society*, Vol. 69 (American Physical Society (APS), 1946) p. 674.

[15] Michael E. Reimer, Gabriele Bulgarini, Nika Akopian, Moïra Hocevar, Maaike Bouwes Bavinck, Marcel A. Verheijen, Erik P.A.M. Bakkers, Leo P. Kouwenhoven, and Val Zwiller, "Bright single-photon sources in bottom-up tailored nanowires," Nature Comm. **3**, 737 (2012).

[16] Gabriele Bulgarini, Michael E. Reimer, Tilman Zehender, Moiïra Hocevar, Erik P. A. M. Bakkers, Leo P. Kouwenhoven, and Valery Zwiller, "Spontaneous emission control of single quantum dots in bottom-up nanowire waveguides," Appl. Phys. Lett. **100**, 121106 (2012).

[17] G. Bulgarini, M. E. Reimer, M. B. Bavinck, K. D. Jöns, D. Dalacu, P. J. Pool, E. P. Bakkers, and V. Zwiller, "Nanowire waveguide launching single photons in a gaussian mode for ideal fiber coupling," Nano Lett. **14**, 4102–4106 (2014).

[18] Adrien Tribu, Gregory Sallen, Thomas Aichele, Régis André, Jean-Philippe Poizat, Catherine Bougerol, Serge Tatarenko, and Kuntheak Kheng, "A high-temperature single-photon source from nanowire quantum dots," Nano Lett. **8**, 4326–4329 (2008).

[19] S. Bounouar, M. Elouneg-Jamroz, M. den Hertog, C. Morchutt, E. Bellet-Amalric, R. André, C. Bougerol, Y. Genuist, J.-Ph. Poizat, S. Tatarenko, and K. Kheng, "Ultrafast room

temperature single-photon source from nanowire-quantum dots," Nano Lett. **12**, 2977 (2012).

[20] Y.-R. Nowicki-Bringuier, R. Hahner, J. Claudon, G. Lecamp, P. Lalanne, and J.-M. Gérard, "A novel high-efficiency single-mode single photon source," Ann. Phys. **32**, 151 (2008).

[21] T. Cremel, M. Elouneg-Jamroz, E. Bellet-Amalric, L. Cagnon, S. Tatarenko, and K. Kheng, "Bottom-up approach to control the photon outcoupling of a II-VI quantum dot with a photonic wire," Phys. Status Solidi C **11**, 1263 (2014).

[22] Julien Claudon, Niels Gregersen, Philippe Lalanne, and Jean-Michel Gérard, "Harnessing light with photonic nanowires: Fundamentals and applications to quantum optics," ChemPhysChem **14**, 2393–2402 (2013).

[23] A. Yariv, *Optical electronics in modern communications* (1997).

[24] Teppo Häyrynen, Jakob Rosenkrantz de Lasson, and Niels Gregersen, "Open-geometry Fourier modal method: modeling nanophotonic structures in infinite domains," J. Opt. Soc. Am. A **33**, 1298 (2016).

[25] A. Vasanelli, R. Ferreira, and G. Bastard, "Continuous absorption background and decoherence in quantum dots," Phys. Rev. Lett. **89** (2002), 10.1103/physrevlett.89.216804.

[26] We note that single-photon emission is preserved if one integrates both the signal from the X and CX lines.[**?**].

[27] Petr Stepanov, Adrien Delga, Xiaorun Zang, Joël Bleuse, Emmanuel Dupuy, Emanuel Peinke, Philippe Lalanne, Jean-Michel Gérard, and Julien Claudon, "Quantum dot spontaneous emission control in a ridge waveguide," Appl. Phys. Lett. **106**, 041112 (2015).

[28] J. D. Eshelby, "The determination of the elastic field of an ellipsoidal inclusion, and related problems," Proc. R. Soc. A **241**, 376–396 (1957).

[29] J. D. Eshelby, "The elastic field outside an ellipsoidal inclusion," Proc. R. Soc. A **252**, 561–569 (1959).

[30] M. Zieliński, "Fine structure of light-hole excitons in nanowire quantum dots," Phys. Rev. B **88**, 115424 (2013).

[31] David Ferrand and Joël Cibert, "Strain in crystalline core-shell nanowires," Eur. Phys. J. Appl. Phys. **67**, 30403 (2014).

[32] K. F. Karlsson, V. Troncale, D. Y. Oberli, A. Malko, E. Pelucchi, A. Rudra, and E. Kapon, "Optical polarization anisotropy and hole states in pyramidal quantum dots," Appl. Phys. Lett. **89**, 251113 (2006).

[33] Catherine Tonin, Richard Hostein, Valia Voliotis, Roger Grousson, Aristide Lemaitre, and Anthony Martinez, "Polarization properties of excitonic qubits in single self-assembled quantum dots," Phys. Rev. B **85**, 155303 (2012).

[34] Mathieu Jeannin, Alberto Artioli, Pamela Rueda-Fonseca, Edith Bellet-Amalric, Kuntheak Kheng, Régis André, Serge Tatarenko, Joël Cibert, David Ferrand, and Gilles Nogues, "Light-hole exciton in a nanowire quantum dot," Phys. Rev. B **95** (2017), 10.1103/physrevb.95.035305.

[35] G. Bacher, R. Weigand, J. Seufert, V. D. Kulakovskii, N. A. Gippius, A. Forchel, K. Leonardi, and D. Hommel, "Biexciton versus exciton lifetime in a single semiconductor quantum dot," Phys. Rev. Lett. **83**, 4417–4420 (1999).

[36] L. Novotny and B. Hecht, *Principles of Nano-Optics*, 2nd ed. (2012).

[37] T. Flissikowski, A. Hundt, M. Lowisch, M. Rabe, and F. Henneberger, "Photon beats from a single semiconductor quantum dot," Phys. Rev. Lett. **86**, 3172 (2001).

[38] Niels Gregersen, Torben R. Nielsen, Julien Claudon, Jean-Michel Gérard, and Jesper Mørk, "Controlling the emission profile of a nanowire with a conical taper," Opt. Lett. **33**, 1693 (2008).

[39] I. Friedler, P. Lalanne, J. P. Hugonin, J. Claudon, J. M. Gérard, A. Beveratos, and I. Robert-Philip, "Efficient photonic mirrors for semiconductor nanowires," Opt. Lett. **33**, 2635 (2008).